Angst, Sebastian; Wolf, Dietrich E.:

Network theory for inhomogeneous thermoelectrics

URN: urn:nbn:de:hbz:464-20161117-102347-0

PURL / DOI: http://dx.doi.org/10.1088/1367-2630/18/4/043004

WWW-Link: http://duepublico.uni-duisburg-essen.de/servlets/DocumentServlet?id=42631

Quelle: New Journal of Physics, Volume 18, April 2016; published 4 April 2016

New Journal of Physics
The open access journal at the forefront of physics

Deutsche Physikalische Gesellschaft DPG
IOP Institute of Physics

Published in partnership with: Deutsche Physikalische Gesellschaft and the Institute of Physics

OPEN ACCESS

RECEIVED
23 December 2015

REVISED
26 February 2016

ACCEPTED FOR PUBLICATION
11 March 2016

PUBLISHED
4 April 2016

PAPER

Network theory for inhomogeneous thermoelectrics

Sebastian Angst and Dietrich E Wolf

Faculty of Physics and CENIDE, University of Duisburg-Essen, D-47048, Duisburg, Germany

E-mail: sebastian.angst@uni-due.de

Keywords: thermoelectrics, inhomogeneous material, Harman method, network model

Abstract

The Onsager–de Groot–Callen transport theory, implemented as a network model, is used to simulate the transient Harman method, which is widely used experimentally to determine all thermoelectric transport coefficients in a single measurement setup. It is shown that this method systematically overestimates the Seebeck coefficient for samples composed of two different materials. As a consequence, the figure of merit is also overestimated, if the thermal coupling of the measurement setup to the environment is weak. For a mixture of metal and semiconductor particles near metal percolation the figure of merit obtained by the Harman method is more than 100% too large. For a correct interpretation of the experimental data, information on composition and microstructure of the sample are indispensable.

1. Introduction

Thermoelectric materials are important for energy harvesting, especially from waste heat [1, 2]. In order to optimize the conversion into electricity, it is desirable to predict device properties by efficient computer simulations. This is one goal of the present paper. More fundamentally, we are going to point out that memory effects render the global response of composite materials, which are common among modern nanostructured thermoelectrics [3], highly complex.

The theoretical description of transport processes goes back to Onsager [4, 5]. Applied to thermoelectrics, this became known as the Onsager–de Groot–Callen theory [6]. A special case is the so-called constant property model (CPM), where the electric and heat conductivity, σ and κ, and the Seebeck coefficient α are assumed to be constant. This model has been studied in detail analytically in one-dimension [7, 8] and will serve as a reference system for validation in this paper.

Since analytic calculations are restricted to simple compounds, numerical models have been developed in order to describe inhomogeneous materials. Although these models are also based on the Onsager–de Groot–Callen theory, most of them do not fully describe the thermoelectric effects, since they do not include Joule heat and/or Peltier heat [9, 10]. They were used to calculate either the heat and electrical conductances or the Seebeck coefficient [11–13]. More complex models [14] exist in the framework of drift-diffusion models, and they are applied e.g. for the simulation of generators in complex geometries [15].

In this paper a simple and coherent way to discretize the Onsager transport theory for thermoelectric materials will be used, which includes all relevant effects and time-dependencies. It can be seen as a version of the finite difference method reviewed in [16]. Originally it was designed for the investigation of transport processes in nano-particle configurations [13, 17, 18], which were mapped to a network model. In this paper it will be applied to disordered bulk systems rather than particle agglomerates.

The model, derived in section 2, enables us to study thermoelectric effects in geometries, which can not be solved analytically. It is validated by comparing simulations and analytical results for one-dimensional segmented CPM thermoelectrics. As an application, the transient Harman method is simulated focusing on inhomogeneous systems like segmented thermoelectrics, superlattices and composite media. Furthermore, we support and extend our findings concerning segmented structures by an analytical treatment.

2. Model

The Onsager–de Groot–Callen theory [8] describes the flow of electrical current density $\mathbf{j}$ and heat current density $\mathbf{j_q}$

$$\mathbf{j} = -\sigma(\nabla\mu/q + \alpha\nabla T), \tag{1}$$

$$\mathbf{j_q} = -\kappa\nabla T + \Pi\,\mathbf{j} \tag{2}$$

driven by the gradients of temperature T and electrochemical potential μ (q is the charge of the mobile particles). According to the Kelvin relation the Peltier coefficient Π is related to the Seebeck coefficient α by $\Pi = \alpha T$. If the Seebeck coefficient is zero, heat and electric transport decouple resulting in Ohm's and Fourier's laws with electrical conductivity σ and heat conductivity κ. Electrochemical potential and temperature are determined by current conservation $\nabla \cdot j = 0$ and volumetric heat production

$$c\dot{T} + \nabla \cdot \mathbf{j_q} = -\frac{\nabla\mu}{q} \cdot \mathbf{j}, \tag{3}$$

with heat capacity per volume, c.

Discretization of these equations in form of a network model is achieved by assigning variable temperatures T_i and electrochemical potentials μ_i to each lattice site i. The bonds between neighboring sites are characterized by an electric conductance G_{ij}, a heat conductance K_{ij}, a Seebeck and a Peltier coefficient, α_{ij} and Π_{ij}. In the network model the electric current I_{ij} and the heat current $I_{\mathrm{q},ij}$ between sites i and j read

$$I_{ij} = G_{ij}\left(\frac{\mu_i - \mu_j}{q} + \alpha_{ij}(T_i - T_j)\right), \tag{4}$$

$$I_{\mathrm{q},ij} = K_{ij}(T_i - T_j) + \Pi_{ij}I_{ij}. \tag{5}$$

The coefficients G_{ij}, K_{ij}, α_{ij}, Π_{ij} depend on the material properties at sites i and j. Let G_i denote the conductance of the material site i. The electrical resistance $1/G_{ij}$ of the bond between sites i and j, half of which is material i or j, respectively, is modeled as

$$\frac{1}{G_{ij}} = \frac{1}{2G_i} + \frac{1}{2G_j} + R \tag{6}$$

with an extra interface contribution R [12]. Likewise, the thermal conductance K_{ij} is calculated from

$$\frac{1}{K_{ij}} = \frac{1}{2K_i} + \frac{1}{2K_j} + R_\mathrm{q}. \tag{7}$$

Being contact rather than material properties, the interface contributions R and R_q are particularly important, if one has only one crystalline material that is divided into grains by grain boundaries. In this paper, however, we want to focus on compound materials, where the different bulk properties have a strong influence on the thermoelectric response. In order not to obscure this bulk effect by the additional influence of the interfaces, we set $R = 0$ and $R_\mathrm{q} = 0$ in the following.

Next, we discuss the Seebeck coefficients α_{ij}, if the materials at the neighboring sites i and j are different. The Seebeck voltage $\alpha_{ij}(T_i - T_j)$ is the sum of two contributions: first, the voltage between site i and the interface in the middle of the bond ij, which is at temperature $T_{c,ij}$, and second, the voltage between the interface and site j:

$$\begin{aligned}\alpha_{ij}(T_i - T_j) &= \alpha_i(T_i - T_{c,ij}) + \alpha_j(T_{c,ij} - T_j)\\ &= \bar{\alpha}_{ij}(T_i - T_j) + \Delta\alpha_{ij}(\bar{T}_{ij} - T_{c,ij}),\end{aligned} \tag{8}$$

where $\bar{\alpha}_{ij} = (\alpha_i + \alpha_j)/2$, $\bar{T}_{ij} = (T_i + T_j)/2$ and $\Delta\alpha_{ij} = (\alpha_i - \alpha_j)$. Approximating $\bar{T}_{ij} = T_{c,ij}$, equation (8) simplifies to

$$\alpha_{ij} = \bar{\alpha}_{ij} = \frac{\alpha_i + \alpha_j}{2}. \tag{9}$$

For the Peltier coefficient Π_{ij}, finally, one has to take the Peltier heat properly into account, which is delivered to or taken from the adjacent materials i and j at the interface. The electrical current I_{ij} carries the heat $\Pi_i I_{ij}$ away from site i and delivers $\Pi_j I_{ij}$ to site j. We assume that the energy difference $(\Pi_i - \Pi_j)I_{ij}$, which is set free (or consumed) at the interface, is given to (or taken from) both adjacent sites in equal parts. The net heat current induced by I_{ij} is then

$$\Pi_{ij}I_{ij} = \Pi_i I_{ij} - \frac{1}{2}(\Pi_i - \Pi_j)I_{ij}, \tag{10}$$

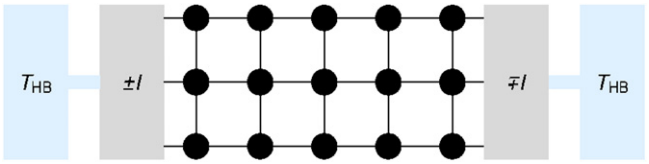

Figure 1. Two-dimensional sketch of setup H. It is composed of the material grid, the electrodes, where electric current I is injected or extracted, and a heat bath (HB) at ambient temperature T_{HB}, coupled to the electrodes via heat conductances K_{HB}.

$$= \Pi_j I_{ij} + \frac{1}{2}(\Pi_i - \Pi_j) I_{ij} \tag{11}$$

with

$$\Pi_{ij} = \frac{\Pi_i + \Pi_j}{2}. \tag{12}$$

Due to the Kelvin relation, $\Pi_i = T_i \alpha_i$ for material i.

For the temporal evolution of the local temperatures, which is essential for the Harman method, the heat capacities C_i must be given for the material belonging to site i. Without specifying the material further, the ratio C/K is the typical time scale, on which temperature differences between neighboring sites are leveled out in the network by heat conduction. On the other hand, the electrical site capacitances C_{el} can be neglected, because the equilibration time C_{el}/G of the electrochemical potential is much shorter than C/K. Therefore it is a reasonable approximation that the electrostatic potential adjusts instantaneously compared to the slow thermal evolution of the system.

The time evolution of temperature T_i is described by a discretization of equation (3), which is given by

$$\dot{T}_i = \frac{1}{C_i} \sum_j \left(-I_{q,ij} + I_{ij} \frac{(\mu_i - \mu_j)}{2q} \right), \tag{13}$$

where j runs over nearest neighbors of i. The electrodes are represented as nodes with one external bond through which heat is exchanged with a heat bath of fixed temperature. The sum over the heat currents between i and j accounts for the divergence of the heat current, while the second term corresponds to Joule heat set free on bond ij. The factor $1/2$ accounts for its delivery in equal parts to sites i and j. For the numerical integration the time step is about one-hundredth of the time scale of the fastest heat exchanging mechanism C/K.

As explained above, the electrochemical potential distribution instantaneously adapts to a temperature change. Thus, the μ_i are obtained by a discretization of $\nabla \cdot \mathbf{j} = 0$, which corresponds to Kirchhoff's first law

$$0 = \sum_j I_{ij}, \tag{14}$$

where j runs over nearest neighbors of i. The electrodes are represented as nodes with one external bond through which a fixed current I is delivered, respectively extracted from the system. Now, the simulation procedure works as follows: an initial temperature distribution and a total current I entering one electrode and leaving the other are provided (see figure 1). The electrochemical potentials are calculated according to equation (14) and then fed into equation (13) in order to calculate the temperatures for the next time step. The temporal evolution of the temperatures implies continuous adjustments of the local currents (according to equation (4)) and hence the electrochemical potentials. Iteratively solving equations (13) and (14) gives the transients and finally the stationary state.

Electrodes are attached to the opposite surfaces normal to the x-axis. They are assumed to have uniform electrochemical potential and temperature. In this paper the electrical current I flowing through the material (and the electrodes) is fixed. Heat losses through lateral surfaces of the transport channel are not taken into account. Two different boundary conditions for the temperature at the electrodes are considered. In sections 3.1 and 3.2 the temperatures $T_0 > T_L = 300$ K of the electrodes at $x = 0$ and $x = L$ are fixed. We denote this as 'setup C'. In the sections starting with section 3.3, a different 'setup H' is used (see figure 1): the electrodes are in contact with the environment, which acts as a heat bath of fixed temperature $T_{HB} = 300$ K. The temperatures of the electrodes are determined by Joule heating, Peltier effect and heat exchange with the environment. In general they differ from T_{HB} and depend on the current direction.

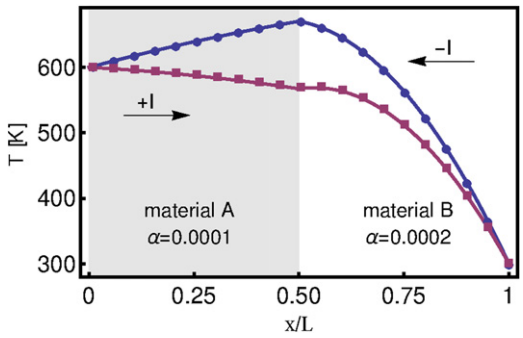

Figure 2. Temperature profile in a layered heterogeneous material calculated as in [19, 20] (lines) and the simulation result (symbols) for $I = -50$ A (points) and $I = 50$ A (squares).

Table 1. The parameters used for the simulations of segmented CPM thermoelectrics. Furthermore we set $T_{\mathrm{HB}} = 300$ K and $K_{\mathrm{env}} = 0.01$ W K^{-1}.

	α (V K^{-1})	σ (S m^{-1})	κ (W (Km)$^{-1}$)
Material A	1×10^{-4}	10^5	2
Material B	2×10^{-4}	10^4	1

3. Application

3.1. Constant property model (CPM)

Here we briefly recall the analytical solution of the one-dimensional CPM [7, 8]. Equations (1)–(3) yield in steady state

$$\frac{\partial^2 T(x)}{\partial x^2} = -\frac{j^2}{\sigma\kappa}, \tag{15}$$

where j represents the x-component of the electrical current density. For fixed temperatures T_0 and T_L the solution reads

$$T(x) = -\frac{j^2}{2\sigma\kappa}x(x-L) + \frac{T_L - T_0}{L}x + T_0. \tag{16}$$

The symmetry of the j^2-term with respect to $x = L/2$ implies that the Joule heat produced in the sample is flowing equally to both electrodes. Similarly, the electrochemical potential profile $\mu(x)$ follows from equations (1) and (16)

$$\frac{\mu(x)}{q} = \frac{\alpha j^2}{2\sigma\kappa}x(x-L) - \left(\frac{j}{\sigma} + \alpha\frac{T_L - T_0}{L}\right)x. \tag{17}$$

Without loss of generality, the integration constant in (17) is $\mu(0) = \mu_0 = 0$.

3.2. Segmented thermoelectrics

Segmented thermoelectrics consist of two layers of different material. If represented by a one-dimensional piecewise CPM, analytic expressions for the temperature and potential profile, as well as for the effective transport coefficients can be obtained [20]. These expressions shall be compared to the corresponding simulation results in order to validate the model presented in section 2.

The analytical calculation makes use of the fact that for each segment equation (15) holds, so that the temperature profile is piecewise parabolic with the respective parameter sets. The six integration constants (for each material two from equation (15) and one from $\partial\mu/\partial x$) are fixed by the boundary conditions T_0, T_L and $\mu_0 = 0$ and by requiring continuity of $T(x)$, $\mu(x)$ and $j_{\mathrm{q},x}(x)$ at the interface.

Figure 2 shows the temperature profile for setup C with the parameters given in table 1. The electrodes are characterized by the same parameters as the adjacent material, which prevents additional Peltier heating/cooling at the electrode-sample interfaces. The size of the sample is $L = L_x = L_y = L_z = 10^{-2}$ m, discretized by $N_y = N_z = 1, N_x = 100$ lattice sites. The current $|I| = 50$ A flows from left to right (squares) or in reverse direction (blue points). The effect of Peltier heating/cooling at the interface can be clearly seen: the temperature

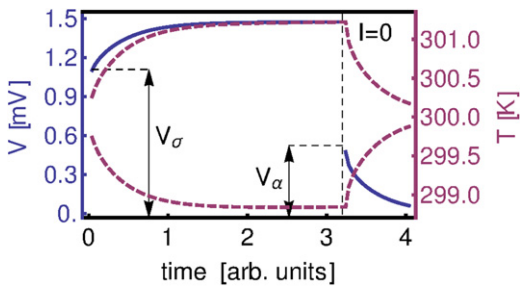

Figure 3. Simulated time-dependency of the voltage between the electrodes (left, solid line) and electrode temperatures (right, dashed lines).

profiles differ significantly for the two current directions. It is this internal temperature profile which affects the results of the Harman method, as will be discussed in section 3.4.

Considering the bond at the interface where $\Delta\alpha_{ij} \neq 0$, we note that equation (9) is an approximationl, if a nonlinear temperature distributions is present. It modifies the total voltage by an interface term, the relative contribution of which vanishes if N_x becomes large. As we discarded interface resistances previously, this interface effect may be neglected as well.

3.3. Harman method

The Harman method [21, 22] is a measurement technique, which allows to determine the three transport parameters and consequently the figure of merit

$$zT = \frac{\alpha^2\sigma}{\kappa}T = \frac{\alpha^2 G_{\text{tot}}}{K_{\text{tot}}}T \tag{18}$$

within one single measurement procedure. Neglecting contact resistances, the conductivities can be replaced by the total electrical conductances G_{tot} and by the total heat conductance K_{tot}, respectively. A setup H as shown in figure 1 is used, and a known dc current I is applied. Due to the Peltier effect one electrode/sample boundary heats up and the other one cools down. At the same time, Joule heating leads to an additional change of the sample temperature. This continues until a steady state is reached, where heat conduction compensates further temperature changes. The time evolution of the electrode temperatures and the voltage across the sample (see figure 3) are measured. After reaching the steady state the current is switched off.

Starting with a homogeneous temperature the electric conductance can be determined from a measurement of the voltage V_σ (see figure 3) via

$$G'_{\text{tot}} = \frac{I}{V_\sigma}, \tag{19}$$

Primed quantities denote Harman method measurement results. In experiments this measurement might be difficult, as the Peltier effect starts immediately creating a temperature difference between the electrodes, when the current is switched on [22]. However, determining G_{tot} during simulations is simpler, since V_σ is recorded before the temperature change affects the voltage. The Seebeck coefficient

$$\alpha' = \frac{V_\alpha}{\Delta T}, \tag{20}$$

is calculated from the temperature difference ΔT and the Seebeck voltage V_α measured immediately after switching off the current I.

The heat conductance of the sample

$$K'_{\text{tot}} = \frac{\alpha'\bar{T} + (\bar{\mu} - \bar{\mu}_{\text{env}})/q}{T_L - T_0}I - \frac{K_{\text{env}}}{2}, \tag{21}$$

is obtained from energy balance in the steady state [22]. Here, K_{env} denotes the heat conductance between the heat bath and the electrodes. The bars indicate averaging of the values at $x = 0$ and $x = L$, e.g. $\bar{T} = (T_0 + T_L)/2$. $\mu_{\text{env},0}$ and $\mu_{\text{env},L}$ are the electrochemical potentials of the leads next to the left and right electrode, respectively.

Let us briefly recall the derivation of (21) according to [22]. The energy current $I_{\text{e}} = I_{\text{q}} + \mu/qI$ arriving at the left electrode from the environment (heat bath or lead) is

$$I_{e,\mathrm{in}}(0) = \frac{\mu_{\mathrm{env},0}}{q} I + K_{\mathrm{env}}(T_{\mathrm{HB}} - T_0) + \frac{I^2}{G_{\mathrm{env}}}. \tag{22}$$

In steady state it must be equal to the energy current

$$I_{e,\mathrm{out}}(L) = \frac{\mu_{\mathrm{env},L}}{q} I + K_{\mathrm{env}}(T_L - T_{\mathrm{HB}}) - \frac{I^2}{G_{\mathrm{env}}}, \tag{23}$$

leaving the sample on the right-hand side. In these expressions, the last terms are the fractions of Joule heat produced in the leads, that flow into the sample. They are assumed to be equal for simplicity. The Peltier coefficient of the (metallic) leads is assumed to be negligibly small. Taking the average of these expressions eliminates the parameters T_{HB} and G_{env}:

$$\bar{I}_e = \frac{\bar{\mu}_{\mathrm{env}}}{q} I + \frac{K_{\mathrm{env}}}{2}(T_L - T_0). \tag{24}$$

On the other hand, the energy current entering the sample from the left must be equal to (22). In the framework of the CPM it is given by

$$I_{e,\mathrm{out}}(0) = \left(\alpha T_0 + \frac{\mu_0}{q}\right) I + K_{\mathrm{tot}}(T_0 - T_L) - \frac{I^2}{2G_{\mathrm{tot}}}, \tag{25}$$

where the subscripts refer to the values at $x = 0$ or $x = L$, respectively, as before. This in turn must be equal to the energy current arriving at the right electrode from the sample

$$I_{e,\mathrm{in}}(L) = \left(\alpha T_L + \frac{\mu_L}{q}\right) I + K_{\mathrm{tot}}(T_0 - T_L) + \frac{I^2}{2G_{\mathrm{tot}}}. \tag{26}$$

Again taking the average of these two expressions eliminates the parameter G_{tot}:

$$\bar{I}_e = (\alpha \bar{T} + \bar{\mu}/q) I - K_{\mathrm{tot}}(T_L - T_0). \tag{27}$$

Identifying this with (24) leads to (21). $(\bar{\mu} - \bar{\mu}_{\mathrm{env}})/q$ is the average contact potential between the electrodes and the leads. Here we do not take contact resistances into account. Hence it does not enter the evaluation of the simulation data. In experiments additional losses due to convection and heat radiation occur, which can be taken into account via correction terms added to equation (21) (e.g. [23]).

The Harman method gives correct results for homogeneous samples. However, as we are going to explain in the next two sections, when applied to heterogeneous systems, it can give values for the Seebeck coefficient, which can be more than 100% off the true value. Consequently, also the heat conductance derived from (21) will be misleading.

3.4. The Harman method applied to segmented thermoelectrics

The basic problem encountered, when the Harman method is applied to inhomogeneous systems, will be explained in this section for the example of a bilayer thermoelectric. We simulated a setup H (figure 1) consisting of materials A and B with parameters given in table 1. The volume fraction of the A-layer is denoted by f. The electrodes are characterized by the same parameters as the adjacent layers. The dimensions are chosen as in section 3.2.

The transport coefficients are obtained by the simulation of the Harman method for different ratios f and currents I. The results are then compared to the analytical expressions, which will be given first.

Denoting the electrochemical potential at the interface betweem the A- and B-segment by μ_{AB}, the electrical conductivity of material A in the absence of a temperature gradient is

$$\sigma_{\mathrm{A}} = \frac{qj\, fL}{\mu_0 - \mu_{\mathrm{AB}}}. \tag{28}$$

The heat conductivity, on the other hand, is defined under open circuit conditions, $j = 0$, as

$$\kappa_{\mathrm{A}} = \frac{j_q\, fL}{T_0 - T_{\mathrm{AB}}}, \tag{29}$$

with the temperature T_{AB} at the interface. The expressions for σ_{B} and κ_{B} read accordingly. The effective electrical and heat conductivities are then derived as a connection in series:

$$\sigma_{\mathrm{eff}} = \frac{qj\, L}{\mu_0 - \mu_{\mathrm{L}}} = \frac{\sigma_{\mathrm{A}}\sigma_{\mathrm{B}}}{\sigma_{\mathrm{A}}(1-f) + \sigma_{\mathrm{B}} f}, \tag{30}$$

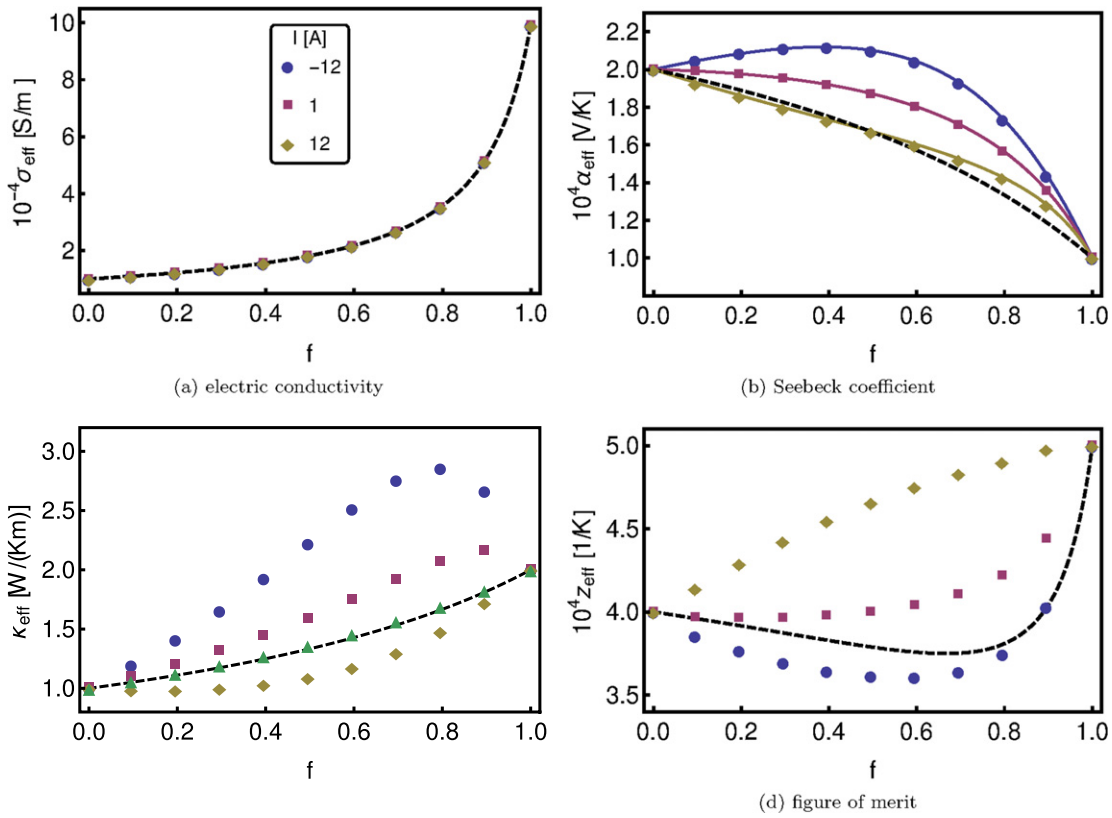

Figure 4. The effective transport coefficients and $z_{\rm eff} = (\alpha_{\rm eff}^2 \sigma_{\rm eff})/\kappa_{\rm eff}$ in dependence of the volume fraction f of material A in a segmented thermoelectric with the parameters of table 1. The dashed lines represent the effective expressions equations (30)–(32), while the dots are obtained from simulations. The solid lines in the upper right figure are analytic results discussed in the text. Green triangles in figure 4(c) are derived according to equation (37), which takes into account the segmented structure (see text).

$$\kappa_{\rm eff} = \frac{j_q\, L}{T_0 - T_{\rm L}} = \frac{\kappa_{\rm A}\kappa_{\rm B}}{\kappa_{\rm A}(1-f) + \kappa_{\rm B} f}. \tag{31}$$

The effective Seebeck coefficient, also defined for open circuit conditions, corresponds to a series connection of the Seebeck voltages created from material A and B:

$$\alpha_{\rm eff} = -\frac{1}{q}\left(\frac{\mu_0 - \mu_L}{T_0 - T_L}\right) = \frac{\kappa_{\rm A}(1-f)\alpha_{\rm B} + \kappa_{\rm B} f \alpha_{\rm A}}{\kappa_{\rm A}(1-f) + \kappa_{\rm B} f}. \tag{32}$$

Figure 4 shows a comparison between equations (30)–(32) and the results of a simulation of the Harman method. As expected, the electric conductivity obtained from the Harman method coincides perfectly with the analytic results (figure 4, upper left). But the Seebeck coefficient (upper right) and the heat conductivity measured via the Harman method depend on the current, which was applied before the measurement of V_α and deviate strongly from the open circuit values, equations (31) and (32). Only in the limiting cases $f \to 1$ and $f \to 0$ the differences vanish. Consequently, the same is true for $z_{\rm eff}$.

Considering the Seebeck coefficient, the deviations arise from the influence of the Peltier heating/cooling at the interfaces on the temperature profile (see figure 5). It causes the current dependence of the temperatures T_0, T_L, $T_{\rm AB}$ and hence of the thermopower

$$V_\alpha = \alpha_{\rm A}(T_{\rm AB} - T_0) + \alpha_{\rm B}(T_L - T_{\rm AB}). \tag{33}$$

If one compares the analytic temperature profiles for $f = 1/2$ created by the external current $I = -12$ A (black, solid line) and $I = 12$ A (gray, solid line) to the respective open circuit profiles (dashed lines) with the same boundary temperatures, a much better agreement, particularly of the interface temperature $T_{\rm AB}$, is found for $I = 12$ A, because Joule heating is nearly compensated by Peltier cooling. This explains, why the effective Seebeck coefficients for $I = 12$ A almost coincide with equation (32), while for $I = -12$ A the Seebeck coefficient is strongly overestimated, since the larger temperature drop is across the material with higher Seebeck coefficient.

Although the Seebeck coefficient is measured at $I = 0$ when using the Harman method, it depends strongly on the previous current (see figure 6), because the temperature profile in inhomogeneous samples acts as a

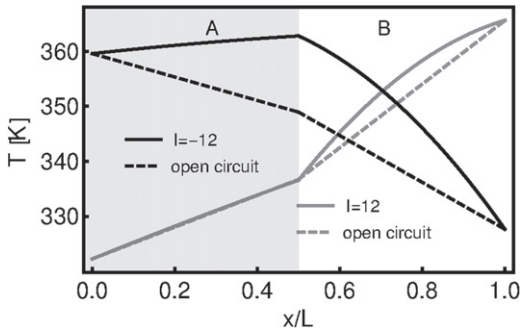

Figure 5. The figure shows the temperature distribution for $f = 0.5$, $I = 12$ A (gray, solid line) and $I = -12$ A (black, solid line). Additionally, the temperature distribution in open circuit conditions are plotted using the same boundary temperatures (dashed lines).

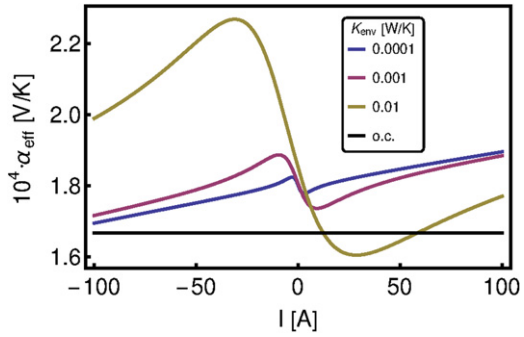

Figure 6. Seebeck coefficient measured with the Harman method for varying currents I and heat coupling K_{env} of a segmented thermoelectric with $f = 0.5$. The black line corresponds to the correct open circuit Seebeck coefficient. As the current approaches $I = 0$ the difference between Harman and open circuit methods does not vanish.

memory. Remarkably, even for arbitrarily small currents $|I|$ the Harman measurement gives a Seebeck coefficient which deviates from the true open circuit value. In this limit Joule heating is negligible and the temperature at all three interfaces depend linearly on the current due to Peltier interface effect. Hence, the relation between the temperature differences across both materials becomes independent of I for $\mathrm{I} \to 0$.

We elaborate this argument by deriving the Seebeck coefficient of a segmented thermoelectric measured by the Harman method analytically. For this purpose we consider the AB structure depicted in figure 7, which is connected to heat bathes with fixed temperature T_{HB} via heat conductance K_{env}. For each segment i the temperature follows

$$T_i(x) = a_i x^2 + b_i x + c_i \quad \text{with} \quad a_i = -\frac{j^2}{2\sigma_i \kappa_i}. \tag{34}$$

Finding the unknown b_i, c_i works basically as discussed in section 3.2, whereby we use a heat flux as boundary conditions here. Note that this procedure can easily be extended to larger number of segments. From $T(x)$ we derive the Seebeck coefficient according to equation (20) using equation (33), which coincides with the simulations (lines in upper right of figure 4). Usually, small currents are applied allowing for a expansion of $T(x)$ around $j = 0$, which leads to

$$\alpha'_{\mathrm{eff}} - \alpha_{\mathrm{eff}} = \frac{(\alpha_{\mathrm{A}} - \alpha_{\mathrm{B}})^2 (1-f) f \left(\kappa_{\mathrm{eff}} + K_{\mathrm{env}} L/(2S)\right)}{\alpha_{\mathrm{eff}} \left((1-f)\kappa_{\mathrm{A}} + f\kappa_{\mathrm{B}}\right)} + \mathcal{O}(j) \tag{35}$$

with the cross section area of the sample S. It is important to note that the difference always has the same sign as α_{eff} meaning that the Harman method systematically overestimates the absolute value of the Seebeck coefficient.

Measuring the heat conductivity according to equation (21) leads to flawed results in a segmented thermoelectric. However, we present a possibility to infer the heat conductivity equation (31) from the Harman method requiring α_{eff}, which can be gained from Harman measurments using equation (35). Basically, we repeat the derivation for K'_{tot} as presented in section 3.3. We determine the energy currents at $x = 0$ and $x = L$

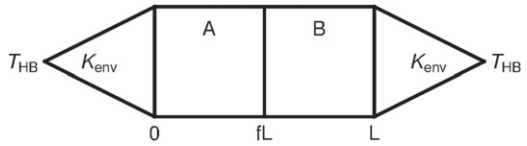

Figure 7. An segmented structure connected to heat bathes of temperature T_{HB} via the heat conductance K_{env}.

using the temperature distribution and its derivative as derived for the strucure depicted in figure 7. The resulting energy currents are expanded to first order around $j = 0$ and their average reads

$$\bar{I}_e = \frac{K_{env}\alpha_{eff}T_{HB}jS}{2K_{tot} + K_{env}} + \frac{\mu_0 + \mu_L}{2q}jS + \mathcal{O}(j^2). \tag{36}$$

Following the arguments of section 3.3 this must be equal to equation (24), which leads to

$$\kappa_{eff} = \frac{\alpha_{eff}T_{HB}L}{(T_L - T_0)}j - \frac{K_{env}L}{2S} + \mathcal{O}(j), \tag{37}$$

where we have set $\mu_0 - \mu_{env,0} = \mu_L - \mu_{env,L} = 0$. Using T_0 and T_L explicitly in equation (24), but not in equation (36) is not inconsistent at all. In fact, we avoid products of the form $(T_0 - T_{HB})j$ or $(T_L - T_{HB})j$, which are of second order in j, since $(T_0 - T_{HB})$ and $(T_L - T_{HB})$ scale with j. The application of equation (37) leads to satisfying agreement as shown by the green triangles in figure 4 (lower left) for $I = 1$ A.

Finally, we discuss z'_{eff} determined by the Harman technique in a segmented thermoelectric for $j \to 0$. Applying equations (30) and (35) and determining the heat conductivity from equation (21) with α'_{eff}, results in

$$z'_{eff} - z_{eff} = \frac{(\alpha_{eff} + \alpha_c)^2 - \alpha_{eff}^2\frac{\kappa_{eff}+\kappa_c}{\kappa_{eff}}}{\kappa_{eff} + \kappa_c}\sigma_{eff} + \mathcal{O}(j) \tag{38}$$

with $\alpha_c = \alpha'_{eff} - \alpha_{eff}$ (see equation (35)) and $\kappa_c = \alpha_c T_{HB}j/(T_L - T_0)$. According to equation (38) the figure of merit may be over or underestimated by the Harman method. Just for $K_{env} \to 0$ we yield

$$z'_{eff} - z_{eff} = \frac{(1-f)f\sigma_{eff}(\alpha_A - \alpha_B)^2}{(1-f)\kappa_A - f\kappa_B} + \mathcal{O}(j) > 0. \tag{39}$$

Hence, for small currents and weak heat coupling the figure of merit is always overestimated by the Harman technique. Considering the relative deviation $\Delta_z = (z'_{eff} - z_{eff})/z_{eff}$ in the limit $K_{env} \to 0$ we find that its maximum occuring at the most unfavorable $f = f_{max}$ is

$$\Delta_z(f_{max}) = \frac{(\alpha_A - \alpha_B)^2}{4\alpha_A\alpha_B}, \tag{40}$$

which is solely affected by the difference of both Seebeck coefficients and can be very large. E.g. for $\alpha_A = 0.0004$ V K^{-1} and $\alpha_B = 0.0001$ V K^{-1} we get $\Delta_z(f_{max}) = 0.5625$ and the Harman method overestimates the z by 56.25%. We conclude that applying the Harman method to segmented structures is tricky and may lead to results that are too optimistic.

Now we show that the systematic error, which we found, if the Harman method is applied to a double-layer system, remains unchanged for periodic superlattices in the limit of weak current. This is particularly easy to see for even numbers of layers. First, for open circuit conditions, a given temperature difference $T_L - T_0$ will be evenly distributed among all N double layers, $T_{\nu+1} - T_\nu = (T_L - T_0)/N$ (see figure 8). In first order this is also the case, if a current is imposed. In particular, the temperature dependence of the Peltier effect may then be neglected. Hence, each double layer has the same systematic error of the effective Seebeck coefficient, equation (35). Consequently the homogeneous array of double layers gives rise to the same error. If the number of layers is odd, this conclusion remains true up to a correction proportional to $1/N$ which vanishes for large superlattices.

Superlattices attracted a lot of interest and a record $zT \approx 2.4$ was measured using the Harman method in Bi_2Te_3/Sb_2Te_3 superlattices [24], which has not been reproduced so far. The individual segments are very thin: Bi_2Te_3 segments have a thickness of 1nm and the Sb_2Te_3 segments have a thickness of 5nm implying $f = 1/6$. Using $\alpha_{BiTe} \approx 2.2 \times 10^{-4}$ V K^{-1} [25], $\alpha_{SbTe} \approx 0.9 \times 10^{-4}$ V K^{-1} [26], $\kappa_{BiTe} \approx 2$ W (Km)$^{-1}$ [27] and $\kappa_{SbTe} \approx 1.8$ W (Km)$^{-1}$ [27] results in $\Delta_z(1/6) \approx 0.18$ corresponding to 18% overestimation of the figure of merit. Note that this result is obtained by a phenomenological theory neglecting quantum and interface effects. Further examples for the application of the Harman method on superlattice structures with potential overestimation of zT can be found in [28–30].

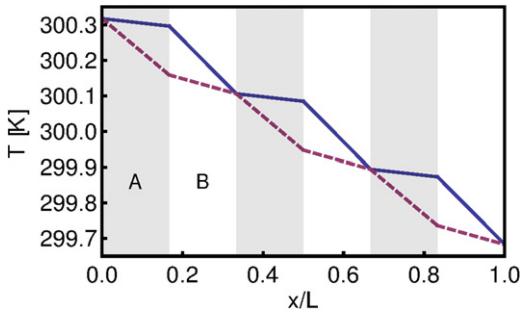

Figure 8. First order temperature distribution (solid line) of a material consisting of $n = 6$ segments and the open circuit temperature distribution (dashed line) with the same boundary temperatures. We used parameters from table 1, except of $\kappa_A = 1$ W (Km)$^{-1}$, $\kappa_B = 3$ W (Km)$^{-1}$ and $K_{env} = 0.1$ W K^{-1}, in order to emphasize the effect discussed in the text.

Table 2. The parameters used for the simulation represent a metal-like (A) and a semiconductor-like (B) material. Furthermore we set $T_{HB} = 300$ K and $K_{env} = 0.01$ W K^{-1}. The system dimensions are as before $L = L_x = L_y = L_z = 0.01$ m.

	σ (S m^{-1})	κ (W (Km)$^{-1}$)	α (V T^{-1})
Material A	1.3×10^5	3	0.0001
Material B	100	1	0.002

3.5. Harman method and composite materials

In this section, random composites made of domains of two different materials are simulated using the network model. The effective transport coefficients are determined from the Harman method, and compared to the ones obtained under open circuit conditions and from an effective medium theory.

Two-dimensional systems are considered with sizes up to 40×40 sites, which are occupied randomly by two different types of domains with metal-like and semiconductor-like transport parameters given in table 2. The fraction f of the metal-like material (A) is varied and for each f at least 10 different randomly chosen configurations were simulated and analyzed.

In contrast to a segmented thermoelectric, the number of interfaces between different materials is large and the error produced by the approximation equation (9) might become relevant. As a test, we make a comparison to a simulation, in which the Seebeck coefficient α_{ij} for a bond between the two materials is determined from α_i and α_j weighted with K_i and K_j as in equation (32). We find that the more sophisticated approximation leads to at most 13% larger values than equation (9). However, we keep equation (9) for the following simulations, as a lower approximation of the error.

For such disordered two-component systems, an effective medium theory was developed [31–33] with the following expression for the Seebeck coefficient:

$$\alpha_{eff} = \alpha_B + (\alpha_A - \alpha_B)\frac{\kappa_{eff}/\sigma_{eff} - \kappa_B/\sigma_B}{\kappa_A/\sigma_A - \kappa_B/\sigma_B}. \tag{41}$$

The effective medium electrical and heat conductivities are given by

$$(1-f)\frac{\sigma_B^{1/t} - \sigma_{eff}^{1/t}}{\sigma_B^{1/t} + A\sigma_{eff}^{1/t}} + f\frac{\sigma_A^{1/t} - \sigma_{eff}^{1/t}}{\sigma_A^{1/t} + A\sigma_{eff}^{1/t}} = 0 \tag{42}$$

and an analogous equation for κ_{eff}. The parameter $A = (1 - f_c)/f_c$ is connected to the percolation threshold f_c.

The Harman method gives an accurate effective electrical conductivity for the composite material, as explained before. By fitting these simulation results with equation (42), we determine the effective medium parameters $f_c = 0.594(2)$ and $t = 1.315(8)$. Note that f_c is close to the expected percolation threshold 0.592 746 for site percolation on a square lattice. The effective medium theory expressions for σ_{eff} and κ_{eff} with the above fitting parameters are fed into equation (41) to obtain the effective medium value for the Seebeck coefficient.

The Seebeck coefficient α'_{eff} obtained by the Harman method deviates strongly from the results for open circuit conditions and from the effective medium theory, especially slightly below the percolation threshold (see figure 9). This phenomenon can be understood by looking at the temperature and current distributions at the moment the Seebeck coefficient is measured. For $f = 0.8$, far above the percolation threshold for the metal-like material, the temperature and current distribution appear homogeneous (see figure 10(a)) leading to a good match of the Harman and the open circuit measurements. In another sample at $f = 0.5$ (see figures 10(b) and

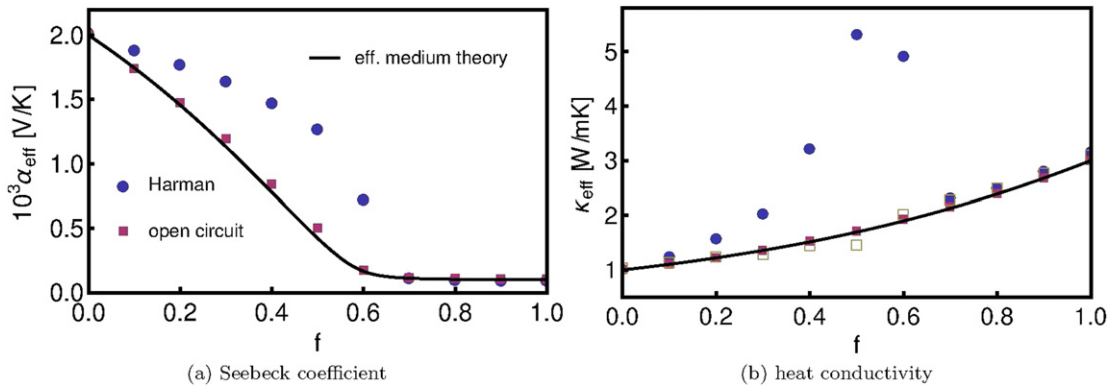

(a) Seebeck coefficient (b) heat conductivity

Figure 9. The Seebeck coefficient and the heat conductivity in dependency of the fraction f of material A. The solid line always represents the corresponding analytic expression, while the dots are simulation results obtained by Harman method (dots) and open circuit measurements (squares). Open squares in figure 9(b) are Harman results using α_{eff} from equation (41).

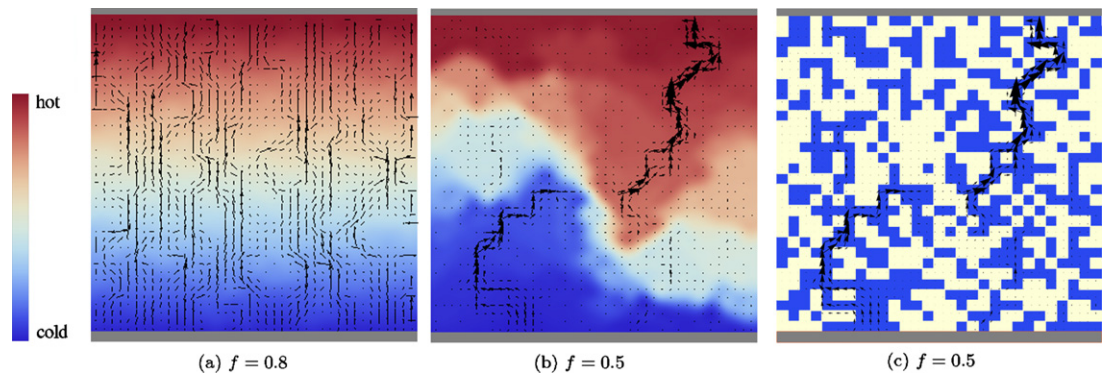

(a) $f = 0.8$ (b) $f = 0.5$ (c) $f = 0.5$

Figure 10. Figures 10(a) and (b) show temperature and current distribution close to ($f = 0.5$) and far from ($f = 0.8$) the percolation threshold for an example setup consisting of 30×30 lattice sites in a Harman setup at the moment of the Seebeck measurement. The electrodes are printed at the bottom and the top of the samples, while the black arrows indicate the strength and the direction of the current. Figure 10(c) shows the particle distribution and blue (dark) squares represent metal-like and yellow (bright) squares represent semi conductor-like material.

(c)), however, a path of well conducting material A almost percolates and thus carries a majority of the current. The percolation is interrupted by material B and a strong Peltier heating/cooling appears. This together with differences in heat conductivity of material A and B results in a strongly inhomogeneous potential and temperature profile. A big part of the temperature drop is located across material B, which is characterized by $\alpha_{\text{B}} > \alpha_{\text{A}}$, hence the effective Seebeck coefficient is enhanced close to the percolation threshold (see figure 9).

The overestimated Seebeck coefficient α'_{eff} in turn affects the heat conductivity shown in figure 9 (right) leading to a an overestimation of κ'_{eff} by a factor larger than 3. Taking α_{eff} determined by equation (41) to derive κ'_{eff} with equation (21) (yellow squares) a significantly better agreement with effective medium theory (black line) is achieved.

4. Summary and conclusion

A simple but powerful simulation model has been derived that describes all thermoelectric responses according to the Onsager–de Groot–Callen transport theory. Although not discussed in the present work we would like to emphasize, that the generalizations to arbitrary (including three-dimensional) lattices and the inclusion of charge dynamics [17] are straight forward.

By means of this model we pointed out that the Harman method to measure the transport coefficients experimentally has substantial systematic errors, when applied to composite materials. In its usual operation mode (weak imposed current, weak thermal coupling to the environment) it always overestimates the absolute value of the Seebeck coefficient and the figure of merit. We gave a numerical example, where the Seebeck coefficient turned out to be wrong by more than a factor of 2 (figure 9, $f \approx 0.5$).

In order to explain this effect, we calculated it analytically for a superlattice of alternating layers of two different materials. The reason is that the Peltier heating/cooling at the interfaces enlarges the temperature difference across the layers with the larger absolute value of the Seebeck coefficient, and reduces it in the other layers. This self organized correlation between Seebeck coefficient and temperature gradient persists, when the current is switched off. The temperature profile acts as a memory of the previous current and affects the thermal voltage, from which the Seebeck coefficient is inferred in the Harman method. The correct Seebeck coefficient would be measured under open circuit conditions for a different internal temperature profile that does not reflect any previous Peltier heating/cooling. The difference between the two measurements of the Seebeck coefficient could be calculated analytically for a superlattice and is given in equation (35). It can be used to correct the Harman measurement.

Overestimating the Seebeck coefficient implies an overestimation of the heat conductivity in the Harman method, as well. However, for small currents we determined an expression, equation (37), which represents the correct open circuit heat conductivity using quantities available during a Harman measurement.

However, our corrections have been derived within the phenomenological Onsager–de Groot–Callen theory, which does not account for quantum effects. Moreover, it neglects the influence of the structure on the phonon contribution to the heat conductivity. To what extent our findings can be recovered in small structures like superlattices with nm sized segments, is an open question. At this point we comment on the neglect of all interface contributions. This is justified as long as the thickness of the homogeneous segments are large compared to $(R_q \kappa)^{-1}$. Note that only the thermal boundary resistance influences the effective Seebeck coefficient. The neglect of heat losses perpendicular to the transport is justified, if the sample is short compared to the cross sectional diameter.

Random composites are only accessible by simulations. In this paper we discussed a material composed of metal and semiconductor particles or domains (figure 10). Below the percolation threshold of the metal-like phase we confirmed that the Harman method overestimates α and κ.

In summary, the application of the Harman method for inhomogeneous media is tricky, and the inhomogeneity of the sample has to be properly accounted for.

Acknowledgments

We thank R Chavez, G Schierning and R Schmechel for valuable discussions. Financial support by the German Research Foundation (DFG) within the Priority Program on nanoscaled thermoelectric materials, SPP 1386 is gratefully acknowledged.

References

[1] Snyder G J and Toberer E S 2008 *Nat. Mater.* **7** 105
[2] Shakouri A 2011 *Annu. Rev. Mater. Res.* **41** 399
[3] Dresselhaus M S, Chen G, Tang M Y, Yang R G, Lee H, Wang D Z, Ren Z F, Fleurial J-P and Gogna P 2007 *Adv. Mater.* **19** 1043
[4] Onsager L 1931 *Phys. Rev.* **37** 405
[5] Onsager L 1931 *Phys. Rev.* **38** 2265
[6] Callen H B 1948 *Phys. Rev.* **73** 1349
[7] Seifert W, Müller E and Walczak S 2006 *ICT '06: 25th Int. Conf. on Thermoelectrics 2006* pp 714–9
[8] Goupil C, Seifert W, Zabrocki K, Müller E and Snyder G J 2011 *Entropy* **13** 1481
[9] Webman I, Jortner J and Cohen M H 1977 *Phys. Rev.* B **16** 2959
[10] Kleber X, Simonet L, Fouquet F and Delnondedieu M 2005 *Model. Simul. Mater. Sci. Eng.* **13** 341
[11] Gather F, Heiliger C and Klar P J 2011 *J. Phys.: Condens. Matter* **23** 335301
[12] Gather F, Heiliger C and Klar P 2011 *Prog. Solid State Chem.* **39** 97
[13] Becker A, Angst S, Schmitz A, Engenhorst M, Stoetzel J, Gautam D, Wiggers H, Wolf D E, Schierning G and Schmechel R 2012 *Appl. Phys. Lett.* **101** 013113
[14] Wachutka G 1990 *IEEE Trans. Comput.-Aided Des. Integr. Circuits Syst.* **9** 1141
[15] Span G, Wagner M, Grasser T and Holmgren L 2007 *Phys. Status Solidi RRL* **1** 241
[16] Hogan T and Shih T 2005 *CRC Thermoelectrics Handbook, Macro to Nano* (Boca Raton, FL: CRC Press)
[17] Hartner S, Schwesig D, Plümel I, Wolf D E, Lorke A and Wiggers H 2012 *Nanoparticles from the Gasphase* (*NanoScience and Technology*) ed A Lorke *et al* (Berlin: Springer) pp 231–71
[18] Angst S, Schierning G and Wolf D E 2013 *AIP Conf. Proc.* **1542** 593–6
[19] Yang Y, Xie S H, Ma F Y and Li J Y 2012 *J. Appl. Phys.* **111** 013510
[20] Müller E, Walczak S and Seifert W 2006 *Phys. Status Solidi* A **203** 2128
[21] Harman T C 1958 *J. Appl. Phys.* **29** 1373
[22] Harman T C, Cahn J H and Logan M J 1959 *J. Appl. Phys.* **30** 1351
[23] Ao X, de Boor J and Schmidt V 2011 *Adv. Energy Mater.* **1** 1007
[24] Venkatasubramanian R, Siivola E, Colpitts T and O'Quinn B 2001 *Nature* **413** 597
[25] Poudel B *et al* 2008 *Science* **320** 634
[26] Mehta R J, Zhang Y, Zhu H, Parker D S, Belley M, Singh D J, Ramprasad R, Borca-Tasciuc T and Ramanath G 2012 *Nano Lett.* **12** 4523
[27] Scherrer H and Scherrer S 2005 *CRC Thermoelectrics Handbook: Macro to Nano* (Boca Raton, FL: CRC Press)

[28] Harman T C, Taylor P J, Walsh M P and LaForge B E 2002 *Science* **297** 2229
[29] Singh R, Bian Z, Zeng G, Zide J, Christofferson J, Chou H-F, Gossard A, Bowers J and Shakouri A 2005 *MRS Proc.* **886** 0886-F04-04
[30] Zeipl R, Jelínek M, Navrátil J, Kocourek T, Leshkov S, Šroubek F, Vaniž J and Walachová J 2013 *Thin Solid Films* **548** 590
[31] McLachlan D S 1987 *J. Phys. C: Solid State Phys.* **20** 865
[32] Bergman D J and Levy O 1991 *J. Appl. Phys.* **70** 6821
[33] Bergman D J and Fel L G 1999 *J. Appl. Phys.* **85** 8205